Sinking of small sphere at low Reynolds number through interface

Duck-Gyu Lee and Ho-Young Kim[a)]
School of Mechanical and Aerospace Engineering, Seoul National University, Seoul 151-744, South Korea

(Received 1 April 2011; accepted 27 June 2011; published online 22 July 2011)

A dense solid sphere gently released on an air-liquid interface slowly sinks into liquid due to gravity, while the motion is resisted by viscous and capillary forces. Here, we predict the sinking velocity of the interface-straddling sphere by a simplified model and experimentally corroborate the results. The viscous drag on the sphere is determined by integrating the surface stress, which is the solution of the Stokes equation, over the wetted area that changes with time. To compute the interfacial tension force that depends on the meniscus profile, we solve the dynamic boundary condition for the normal and tangential stresses at the air-liquid interface. The predicted sinking velocity, a function of the sphere density and radius, liquid density, viscosity and surface tension, and the dynamic contact angle, is in good agreement with the experimental measurements except for the late stages when meniscus snapping occurs. We also construct a scaling law for the steady velocity of a sinking sphere, which gives the characteristic sinking time. © *2011 American Institute of Physics*. [doi:10.1063/1.3614536]

I. INTRODUCTION

A completely immersed solid sphere that is denser than the surrounding liquid falls due to gravity and its steady velocity is determined by the balance of the negative buoyant force with the drag. When the Reynolds number defined as $\mathrm{Re} = \rho_f Ua/\mu \ll 1$, where U is the sphere velocity, a the sphere radius, and ρ_f and μ the liquid's density and viscosity, respectively, the drag $F_D = 6\pi\mu Ua$, then the terminal velocity is simply given by $U_t = \frac{2}{9}(\rho_s - \rho_f)a^2 g/\mu$, where ρ_s is the solid density and g the gravitational acceleration. Now, we consider a tiny dense solid sphere initially released upon the liquid's free surface. For the partially submerged solid object, the interfacial tension in addition to the hydrostatic pressure and viscous stresses exerts force on the object, whose direction is determined by the contact angle and the object elevation with respect to the unperturbed free surface, h.[1,2]

Although how small (even flexible) objects can float in equilibrium at an interface is well understood now,[3,4] the question of how an object sinks if the subtle balance of forces is upset has drawn scientific interests only recently. This can happen if the solid weight exceeds the vertical force, which surface tension and hydrostatic pressure provide, due to the increased solid density or wettability or to the reduced interfacial tension. In addition to our mundane observations of flour of salt and sugar falling into water when cooking, this problem has implications in an industrial mineral-separation process called flotation.[5] In the world of tiny aquatic arthropods such as water striders[6] and fishing spiders[7] and insects captured by carnivorous pitcher plants,[8] to drown or not is a matter of life and death. Motivated by a water strider leg being drowned on surfactant-added water, Vella *et al.*[9] considered the sinking of a dense cylinder as it is gently placed on the air-water interface. The liquid flow was assumed to be potential due to the high Reynolds number, the meniscus shape was obtained by solving the two-dimensional Young-Laplace equation, and the pressure around the cylinder was taken to be hydrostatic. Vella and Li[10] studied the impulsive motion of a small cylinder floating horizontally at the liquid-gas interface, suggesting that the influence of contact line may be important in the transition from floating to sinking. Duez *et al.*[11] showed that the water repellency plays an important role in making an air cavity upon impact of a sphere and gave conditions of the impact velocity and contact angle for the air cavity to form. Aristoff and Bush[12] investigated the water entry dynamics of small hydrophobic spheres with a major focus on understanding the inviscid collapse dynamics of cavity made by an impactor. Lee and Kim[13] showed that a tiny superhydrophobic sphere impacting on water may penetrate, bounce off, or oscillate on the free surface depending on the impact conditions, i.e., the relative magnitude of impact inertia to surface tension.

An object that sinks into a liquid eventually gets fully immersed, at which instant the object loses its contact with the meniscus. Such physical process of the meniscus detachment is commonly observed in a classical mineral separation process[14] and in biological locomotion of aquatic animals.[6] The interface failure problem was studied in various contexts including the breakup of the liquid film with a hole,[15] the failure of a liquid bridge between plates that move apart from each other,[16] and the disengagement of a horizontal cylinder that is lifted off a liquid surface.[17] A common observation is that the liquid interface becomes unstable near the detachment leading to a sudden burst, so that the theoretically computed meniscus profile abruptly stops matching experiment.[18,19]

To obtain a basic understanding of the dynamics of partially submerged sinking sphere, we begin with dimensional analysis. When a solid sphere sinks into an air-liquid interface, the liquid exerts various forces on the sphere arising from the hydrodynamic ($\sim \rho_f \dot{h}^2 a^2$) and hydrostatic ($\sim \rho_f g h a^2$) pressure, added inertia ($\sim \rho_f \ddot{h} a^3$), viscous

a)Author to whom correspondence should be addressed. Electronic mail: hyk@snu.ac.kr. Tel.: 82-2-880-9286. Fax: 82-2-880-9287.

($\sim \mu \dot{h} a$), and surface tension ($\sim \gamma a$) effects, where $\dot{h} = \mathrm{d}h/\mathrm{d}t$ with t being time and γ is the surface tension. Dimensional analysis leads to the following relationship:

$$\frac{h}{l_c} = f(\tau; D, \mathrm{Bo}, \mathrm{Ca}, \mathrm{Re}, \theta), \tag{1}$$

where the capillary length $l_c = \sqrt{\gamma/\rho_f g}$, the nondimensional time $\tau = t\gamma/(\mu a)$, the density ratio $D = \rho_s/\rho_f$, the Bond number $\mathrm{Bo} = \rho_f g a^2/\gamma$, the Capillary number $\mathrm{Ca} = \mu U/\gamma$, the Reynolds number $\mathrm{Re} = \rho_f U a/\mu$, and θ is the dynamic contact angle. Unlike the fully immersed sphere of which behavior is determined by D and Re only, the motion of a partially submersed sphere additionally depends on the parameters related to wetting. Here, we are interested in predicting the velocity of a small solid sphere straddling a liquid-gas interface corresponding to $\mathrm{Re} \ll 1$ and $\mathrm{Bo} \ll 1$ and corroborate the theoretical results experimentally.

II. THEORETICAL FORMULATION AND EXPERIMENTS

A. Hydrodynamic model

We consider a solid sphere sinking with a velocity $U = -\dot{h}$, where h denotes the elevation of the sphere's center with respect to the unperturbed free surface through a viscous liquid as shown in Fig. 1. When $\mathrm{Re} \ll 1$ and $\mathrm{Bo} \ll 1$, the added inertia and the form drag are negligibly small compared to the viscous force, while the buoyancy can be neglected compared to the surface tension force only when $h \sim a$. Thus, the equation of motion of the solid sphere is written as

$$\frac{4}{3}\pi a^3 \rho_s \ddot{h} = F_d + F_b + F_s - F_w, \tag{2}$$

where F_d is the viscous drag, F_b the buoyancy, F_s the surface tension force, and F_w the solid weight.

To determine F_d and F_b, we need to solve the flow field around the sphere and determine the location and shape of the meniscus. To enable the analytical formulation of this problem instead of numerically solving the flow field with a deforming meniscus, we start with a classical solution of Stokes,[20] which is strictly valid for the sinking of a completely immersed sphere surrounded by a liquid of infinite extent. Since $\mathrm{Re} \ll 1$, the flow induced by a sinking sphere

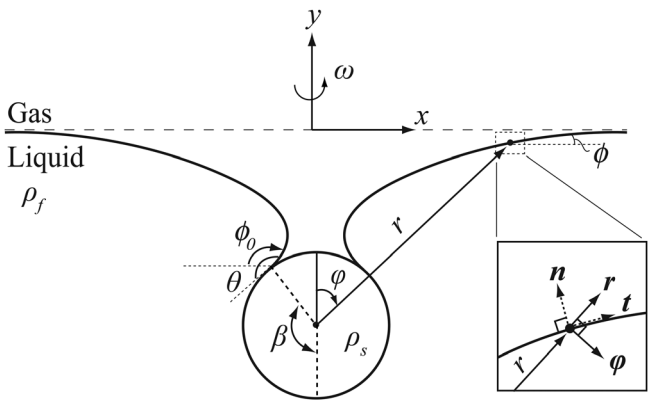

FIG. 2. Geometry of a sphere straddling the gas-liquid interface.

is inertia free, so that the stream function ψ satisfies $\mathcal{D}^2(\mathcal{D}^2\psi) = 0$, where

$$\mathcal{D}^2 \equiv \frac{\partial^2}{\partial r^2} + \frac{\sin\varphi}{r^2}\frac{\partial}{\partial\varphi}\left(\frac{1}{\sin\varphi}\frac{\partial}{\partial\varphi}\right). \tag{3}$$

Here, ψ is such that $u_r = (\partial\psi/\partial\varphi)/(r^2 \sin\varphi)$ and $u_\varphi = -(\partial\psi/\partial r)/(r \sin\varphi)$, where u is the velocity in the direction designated by its subscript and (r, φ, ω) is a spherical coordinate system as shown in Fig. 2. For a flow around a falling sphere, the stream function is given by $\psi = -\frac{1}{4}\dot{h}a^2(a/r - 3r/a)\sin^2\varphi$. Then, we get $u_r = \dot{h}(-\frac{1}{2}a^3/r^3 + \frac{3}{2}a/r)\cos\varphi$ and $u_\varphi = -\dot{h}(\frac{1}{4}a^3/r^3 + \frac{3}{4}a/r)\sin\varphi$. Substituting these velocity components into the following Stokes equations:

$$\begin{aligned}\frac{\partial p}{\partial r} &= \mu\left(\nabla^2 u_r - \frac{2u_r}{r^2} - \frac{2}{r^2}\frac{\partial u_\varphi}{\partial\varphi} - \frac{2u_\varphi \cot\varphi}{r^2}\right) - \rho_f g\cos\varphi,\\ \frac{1}{r}\frac{\partial p}{\partial\varphi} &= \mu\left(\nabla^2 u_\varphi + \frac{2}{r^2}\frac{\partial u_r}{\partial\varphi} - \frac{u_\varphi}{r^2\sin^2\varphi}\right) + \rho_f g\sin\varphi,\end{aligned} \tag{4}$$

subject to the condition $p = p_a - \rho g y$ as $r \to \infty$ yields a pressure distribution around the sinking sphere as

$$p(r, \varphi) = p_a + \frac{3\mu a\dot{h}\cos\varphi}{2r^2} - \rho_f g y, \tag{5}$$

where p_a is the atmospheric pressure and $y = h + r\cos\varphi$. Now, we assume that the real flow field in the liquid around the sinking sphere, which is partially exposed to air, is not changed substantially from the foregoing theoretical field.

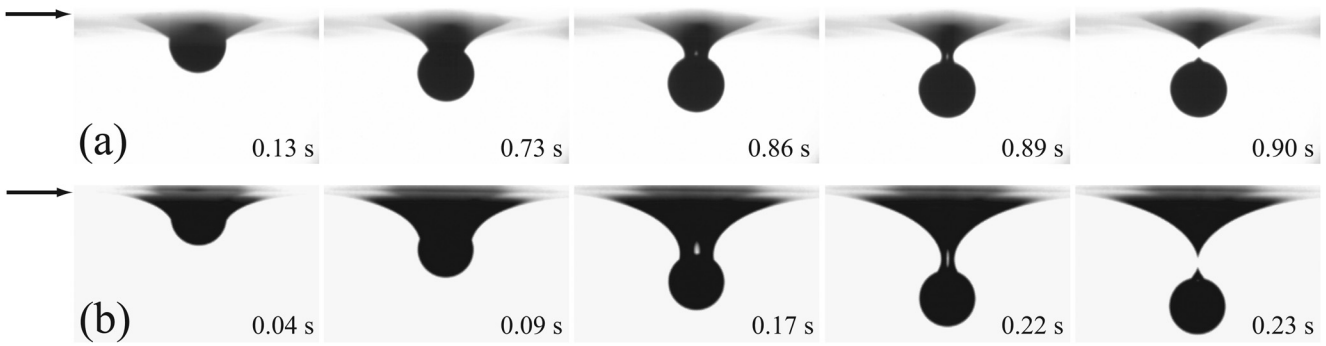

FIG. 1. Images of spheres with the radius 0.75 mm sinking vertically through the surfaces of (a) glycerine and (b) silicone oil. (a) $\mathrm{Re} = 0.011$, $D = 11.0$, and $\mathrm{Bo} = 0.11$. (b) $\mathrm{Re} = 0.038$, $D = 14.9$, and $\mathrm{Bo} = 0.25$. The horizontal arrows indicate the elevation of the undisturbed free surface.

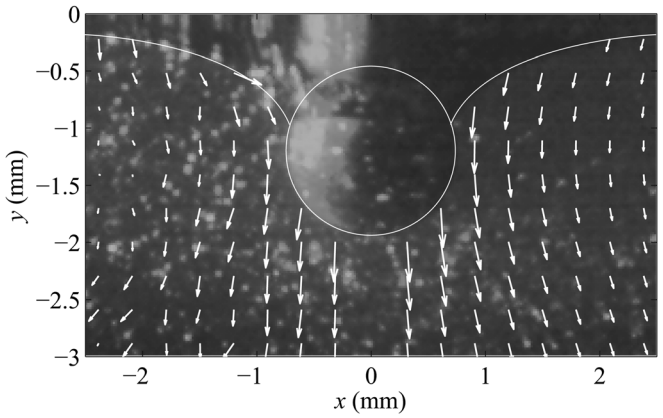

FIG. 3. The velocity field around a sphere with $a = 0.75$ mm in silicone oil at $t = 0.084$ s. The velocity vectors in the domain $x < 0$ are the empirically obtained results using particle image velocimetry. The vectors in the region $x > 0$ are the solutions of the Stokes equation.

Figure 3 compares the velocity field obtained by a particle image velocimetry (PIV) experiment and the theoretical field. Except that the velocity normal to the interface is zero in reality, the theoretically approximated velocity vectors appear to closely simulate the experimental measurements.

The pressure on the wet surface of the sphere, where $r = a$ and $\pi - \beta < \varphi < \pi$, is then given by

$$p(a, \varphi) = p_a + \frac{3\mu\dot{h}\cos\varphi}{2a} - \rho_f g(h + a\cos\varphi). \tag{6}$$

Now, we can calculate the vertical component of the pressure force acting on the sphere by integrating the pressure over the wet area,

$$\begin{aligned} F_p &= -\int_{\pi-\beta}^{\pi} \pi a^2 (p - p_a)\sin(2\varphi)\mathrm{d}\varphi \\ &= \pi\mu\dot{h}aA(\beta) + 2\pi a^2\rho_f gB(\beta), \end{aligned} \tag{7}$$

where $A(\beta) = \cos^3\beta - 1$ and $B(\beta) = \frac{1}{2}h(\cos^2\beta - 1) + \frac{1}{3}a(1 - \cos^3\beta)$. The first term on the right-hand side of Eq. (7) corresponds to the hydrodynamic pressure force, and the second term the buoyancy F_b. Integrating the vertical component of shear stresses over the solid surface area in contact with liquid gives the viscous force F_μ as

$$\begin{aligned} F_\mu &= -\int_{\pi-\beta}^{\pi} 2\pi a^2 \tau_{r\varphi}\sin^2\varphi\mathrm{d}\varphi \\ &= \pi\mu\dot{h}a(-2 + 3\cos\beta - \cos^3\beta). \end{aligned} \tag{8}$$

The total force due to liquid flow can be recombined as $F_p + F_\mu = F_d + F_b$, so that the force of the viscous origin F_d and the buoyancy F_b is, respectively, given by

$$F_d = F_\mu + \pi\mu\dot{h}aA(\beta) \tag{9}$$

and

$$F_b = 2\pi a^2\rho_f gB(\beta). \tag{10}$$

We note that when $\beta = \pi$, corresponding to the fully immersed sphere, F_d becomes the classical Stokes drag: $F_d = 6\pi\mu Ua$.

The vertical component of the surface tension force F_s that acts tangent to the interface along the contact line is given by

$$F_s = 2\pi a\gamma\sin\beta\sin\phi_0, \tag{11}$$

where the slope of the meniscus at the contact line $\phi_0 = \theta + \beta - \pi$. Substituting those forces and $F_w = \frac{4}{3}\pi a^3\rho_s g$ into Eq. (2) gives a second-order differential equation for h once the values of θ and β are determined. In general, the dynamic contact angle θ is dependent on the combination of three phases of liquid-solid-gas and the sinking velocity. An extent of sphere submersion, $\beta(t)$, can be obtained only after the interface profile is theoretically determined with time. In the following, we find a relationship between θ and β by solving the meniscus shape at low Re.

B. Interface profile at low Reynolds numbers

A balance of stresses at the boundary of two fluids can be expressed as[21]

$$e_{ij}t_i n_j = 0 \tag{12}$$

in the tangential and

$$\kappa = \frac{p_a - p}{\gamma} + \frac{2\mu}{\gamma}e_{ij}n_i n_j \tag{13}$$

in the normal direction to the boundary, where e_{ij} is the strain rate tensor, $e_{ij} = \frac{1}{2}(\partial u_i/\partial x_j + \partial u_j/\partial x_i)$, and n and t are the normal and tangential unit vectors, respectively. The curvature at a given point of the interface, $\kappa = \cos\phi(\mathrm{d}\phi/\mathrm{d}x) + \sin\phi/x$ in the axisymmetric fluid interface. We expand Eq. (12) as $(e_{rr}n_r + e_{r\varphi}n_\varphi)n_\varphi = (e_{r\varphi}n_r + e_{\varphi\varphi}n_\varphi)n_r$ using the relations $t_r = -n_\varphi = \sin(\phi + \varphi)$ and $t_\varphi = n_r = \cos(\phi + \varphi)$. In Eq. (13), we write $e_{ij}n_i n_j = (e_{rr}n_r + e_{r\varphi}n_\varphi)n_r + (e_{r\varphi}n_r + e_{\varphi\varphi}n_\varphi)n_\varphi$ and use the expanded form of Eq. (12) to get

$$e_{ij}n_i n_j = -e_{r\varphi}\cot(\phi + \varphi) + e_{\varphi\varphi}, \tag{14}$$

where $e_{r\varphi} = \frac{3}{4}\dot{h}a^3r^{-4}\sin\varphi$ and $e_{\varphi\varphi} = \frac{3}{4}\dot{h}(-a^3r^{-4} + ar^{-2}) \times\cos\varphi$. Using the pressure distribution around the meniscus as given by Eq. (5), Eq. (13) that describes the dynamic meniscus profiles becomes

$$\begin{aligned} \frac{\mathrm{d}x}{\mathrm{d}\phi} &= \left\{-\frac{\tan\phi}{x} + \frac{y}{l_c^2\cos\phi} + \frac{3a^3\mathrm{Ca}}{2r^4\cos\phi}[\sin\varphi\cot(\phi+\varphi) + \cos\varphi]\right\}^{-1}, \\ \frac{\mathrm{d}y}{\mathrm{d}\phi} &= \tan\phi\frac{\mathrm{d}x}{\mathrm{d}\phi}. \end{aligned} \tag{15}$$

The boundary conditions are such that

$$\begin{aligned} &x = a\sin\beta \quad \text{and} \quad y = h - a\cos\beta \quad \text{at} \quad \phi = \phi_0, \\ &y \to 0 \quad \text{and} \quad x \to \infty \text{ as } \phi \to 0. \end{aligned} \tag{16}$$

To solve this system, we make an initial guess for β and integrate Eq. (15) to $x = L$, where we require $\tan\phi|_{x=L} < 10^{-3}$. Then, we check whether the following convergence criterion is met: $y(L)/l_c < 10^{-3}$. By repeating this process with a renewed initial guess for β until the criterion is met, we solve the interface profile and $\beta(t)$, which in turn gives us the location of the sphere in the next step.

TABLE I. Physical properties of the liquids.

Liquid	ρ_f (kg/m^3)	γ (mN/m)	μ (kg/m/s)
Glycerine	1260	63.3	1.54
Silicone oil	968	21.1	1.06
Water	998	72.8	1.0×10^{-3}

C. Experiments

We gently released a small but heavy sphere onto the free surface of a viscous liquid and observed the temporal evolution of the sphere location and the meniscus shape. We used tungsten spheres of the radius ranging between 0.4 and 1.0 mm and of the density 15 000 kg m^{-3}. Aqueous 99% glycerine and silicone oil were used as the viscous liquids, whose properties (with those of water for comparison) are listed in Table I. It is noted that the surface tension of glycerine is about three times larger than that of silicone oil, although its viscosity is only 50% higher than that of silicone oil, which allows us to efficiently reveal the effects of the surface tension on the sinking process. Prior to the experiments with glycerine, the spheres were spray-coated with nitrocellulose lacquer to attain a static contact angle of 92°. The spheres to sink in silicone oil were ultrasonically cleaned in acetone and in methanol both for 5 min, and the static contact angle was measured to be 21°. To minimize the initial impact speed of the sphere, we released the sphere that was initially adhered to an electromagnet by turning the magnet off as the sphere touches the free surface. The measurement of the sphere velocity started as the bottom of the sphere passed through a blurred region around the free surface (See Fig. 1). In our experiments, the Reynolds number based on the initial sinking speed, which also corresponds to the maximum speed, ranged between 0.02 and 0.07, so that the creeping flow assumption is satisfied. The sphere location and the meniscus shape were observed through the side of a transparent acrylic bath (50 mm × 50 mm × 60 mm) via a high speed camera (Redlake HS-4) recording images at a rate of 500 s^{-1}. Then the images were analyzed to determine the height of the sphere with respect to the undeformed free surface. For the PIV experiment to visualize liquid flows around the sinking sphere, the liquid was seeded with hollow glass spheres with 10 μm and 1100 kg/m^3 in diameter and density, respectively, which were illuminated by a 2-W semiconductor laser focused into a light sheet approximately 0.3 mm thick. The same high speed camera as above recorded the motion of the seeds as well as the sinking sphere.

III. RESULTS AND DISCUSSION

A. Comparison of theory and experiment

Figure 4 compares the experimentally measured temporal evolution of h of the spheres with $a = 0.75$ mm to its theoretical predictions obtained by solving Eq. (2). We used experimentally measured dynamic contact angle θ in our theory, so that $\theta = 128°$ for $0 < t < 0.10$ s and $\theta = 112°$ for $t > 0.10$ s in (a), and $\theta = 149°$ for all t in (b). Line I is the result of solving β as a function of time via Eq. (15). We also find β using the Young-Laplace equation that assumes

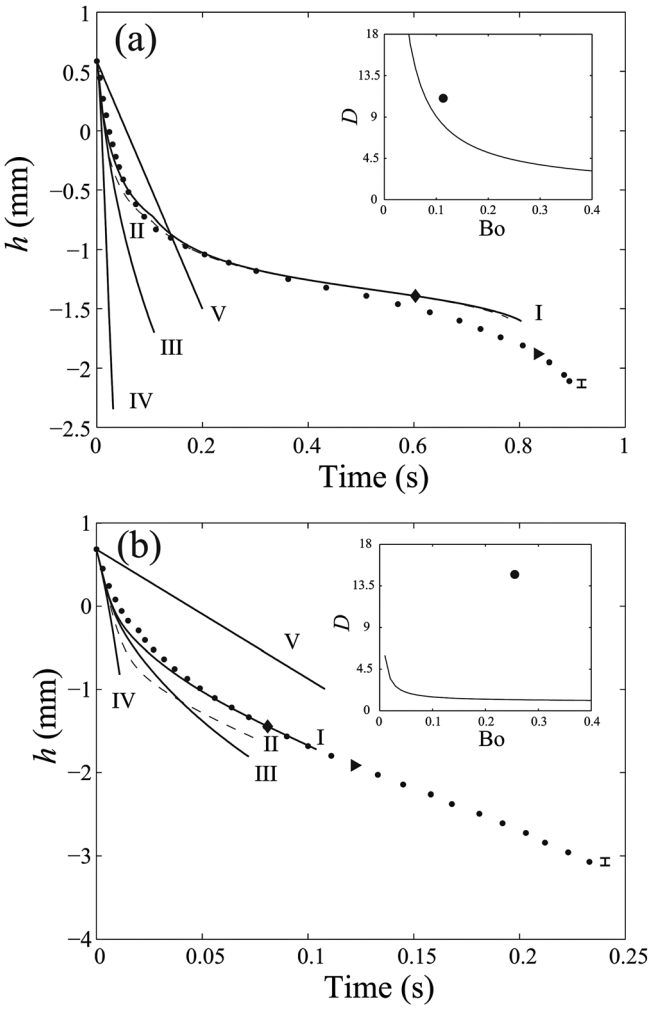

FIG. 4. Comparison between the theoretical predictions and the experimental results of h versus time: (a) glycerine and (b) silicone oil. Insets show the maximum density ratio of a sphere that can be supported on each liquid in equilibrium as a function of Bo (solid line) and the actual experimental condition (filled circle). Characteristic error bars are shown next to the rightmost experimental points.

$\mathrm{Ca} = 0$, which gives $h(t)$ as a dashed line II. Lines III and IV are obtained by neglecting the surface tension force F_s and the viscous force F_d, respectively, in Eq. (2). In Fig. 4(a), both the lines I and II agree well with the experimental measurements, whereas only line I matches well with experiment in (b). The results show that our simplified analytical theory using Eq. (2) can predict the sinking velocity of a sphere into a viscous liquid with a high accuracy up to a point where the calculation ceases for the reason that will be discussed later. The large deviations of the lines III and IV from the measurement results quantitatively reveal the roles of the surface tension and the viscosity in the slow sinking of the sphere. Line V corresponds to the case when the sphere sinks as if completely immersed in the liquid with the terminal velocity U_t. We detail the foregoing observations in what follows.

Although the spheres of the identical radius and density were used and the dynamic contact angles were similar, different liquid properties led to different D and Bo; thus, significant difference is noted between the sinking behaviors of Figs. 4(a) and 4(b). In (a), following the rather rapid initial descent of the sphere due to a limited contact area with the

resisting liquid, the sinking is significantly retarded while no such retardation is noted in (b). The strong resistance to the sinking of a partially immersed ($\sim 107^\circ < \beta < \sim 147^\circ$ for $0.2\,\text{s} < t < 0.8\,\text{s}$) sphere in (a) implies that the upward force provided by the surface tension and the buoyancy can nearly balance the solid weight. To compare the load supporting capacity of the liquids, we plot the maximum value of the density ratio D of a sphere that can be supported on each liquid in equilibrium as the function of Bo in the insets of Fig. 4 using the theory of Vella *et al.*[2] We see that the sphere sinking in glycerine has the density ratio much closer to the maximum value that can be statically supported than the sphere in silicone oil. Hence, as the sphere sinks to approach the height where the supporting force of the liquid interface is maximized, the sinking is significantly retarded and the floatation is prolonged in Fig. 4(a). When β further increases, the vertical component of the capillary force is now decreased due to the reduced contact line length and the deviation of ϕ_0 from $\pi/2$; thus, the sinking velocity increases as shown for $t > 0.8\,\text{s}$ in (a).

In Fig. 4(b), the load bearing capacity of the silicone oil is not sufficient to significantly retard the sinking sphere because the density of the sphere is much higher than that can be statically supported. Therefore, the sinking velocity is higher than that on glycerine, leading to the increased contribution of the viscous force. Such tendency can be quantitatively checked in Fig. 5, which plots the contribution of each force component exerted on the sinking spheres of Fig. 4 with time. While the surface tension force F_s dominates over the viscous drag F_d in (a), F_d is greater than F_s in (b) implying that the Young-Laplace equation falls far from accurate in this case. This is why line II shows discernible difference from line I in Fig. 4(b). Line III of Fig. 4(a) shows a greater discrepancy from line I than that of (b), corresponding to the dominant role of F_s in retarding the sinking sphere of (a). The kinks in Fig. 5(a) are due to the sudden change in θ at $t = 0.10\,\text{s}$ as described above.

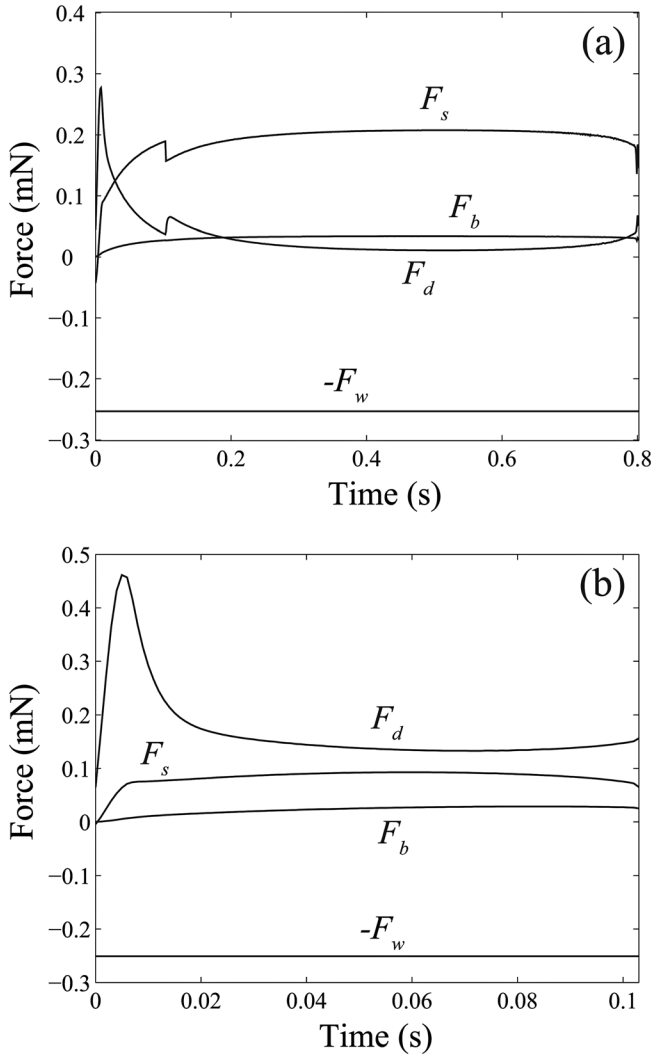

FIG. 5. Contribution of each force component exerted on a sinking sphere: (a) glycerine and (b) silicone oil.

B. Meniscus snapping

Now, we turn to the late stages of sphere sinking. In Figs. 4(a) and 4(b), the sphere is experimentally observed to sink completely or to lose contact with air at $t = 0.89\,\text{s}$ and 0.23 s, respectively. However, our theoretical calculation, i.e., line I, stops at around $t = 0.80\,\text{s}$ and 0.10 s, respectively. We refer to the time until which the theoretical prediction of the sphere location is possible as t_c. We stop computation at t_c because physically reasonable values of β are no longer obtained beyond t_c. Figure 6 plots β versus h that are measured and theoretically calculated even beyond t_c. In the experiments, h decreases (the sphere descends) leading to the increase of β (the meniscus climbing up the sphere). On the other hand, a theoretical relationship between h and β based on Eq. (15) predicts that β increases despite the increase of h when $t > t_c$, which is physically unacceptable. We scrutinized the shape evolution of the meniscus to understand what happens near t_c. Figure 7(a) shows two vertical locations of the meniscus η_1 and η_2, which, respectively, correspond to the elevation of the contact line and the point where the line $x = 1.5a$ intersects with the meniscus. We measured the temporal evolution of these positions. The results, Fig. 7(b), show that the contact line (η_1) monotonically descends along the fall of the sphere. However, the meniscus far from the contact line (η_2) initially descends (time range A) but stops descending at $t = 0.11\,\text{s}$ but rather plateaus until $t = 0.15\,\text{s}$ (time range B), and then slightly rises (time range C). The temporal evolutions of the experimentally obtained meniscus shapes in each time range are shown in Fig. 7(c). The descent of the contact line despite the stationary meniscus of far field in time range B suggests that the meniscus near the sphere gets stretched. We note that the moment η_2 starts plateau matches t_c at which the theoretical prediction of the meniscus stops being possible, implying that the interface stretching cannot be treated with the current model.

A few attempts were made previously to predict the instant when the meniscus touching the solid surface snaps. Vella[3] assumed that a cylinder completely sinks when ϕ_0 becomes $\pi/2$. Lee and Kim[17] postulated that the meniscus is detached from a solid object that is lifted off the interface when the free energy of the system equals that of the detached state. For details of the free energy analysis, see the Appendix. We employed both the conditions and marked the

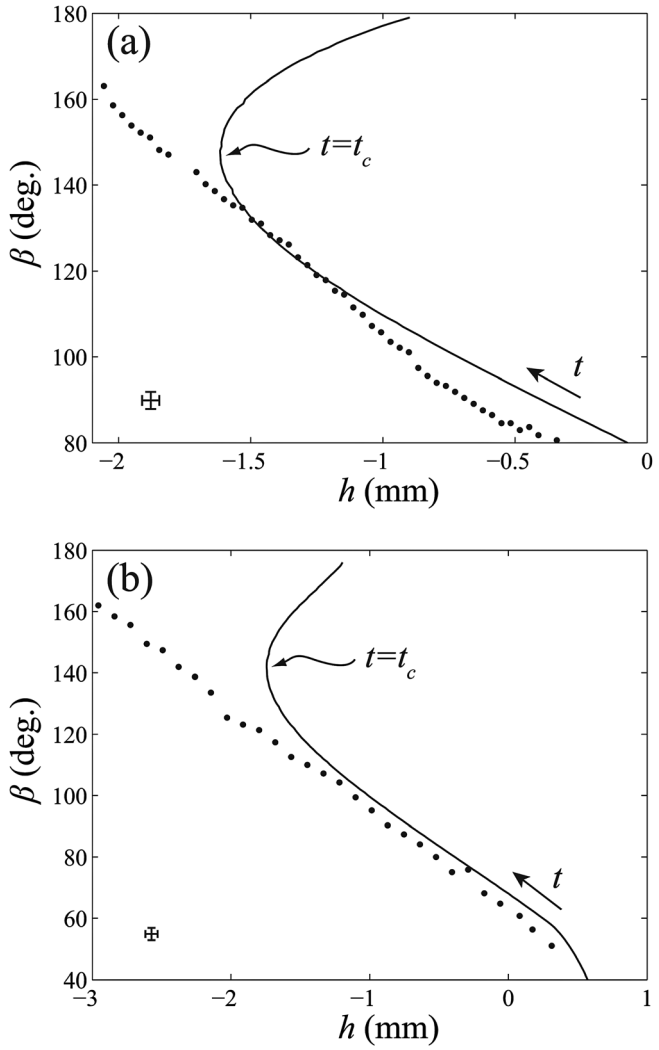

FIG. 6. The evolutions of β and h with time. The circles correspond to experimental measurements and the solid line is the solution of Eq. (15). (a) Glycerine. (b) Silicone oil. Characteristic error bars are shown.

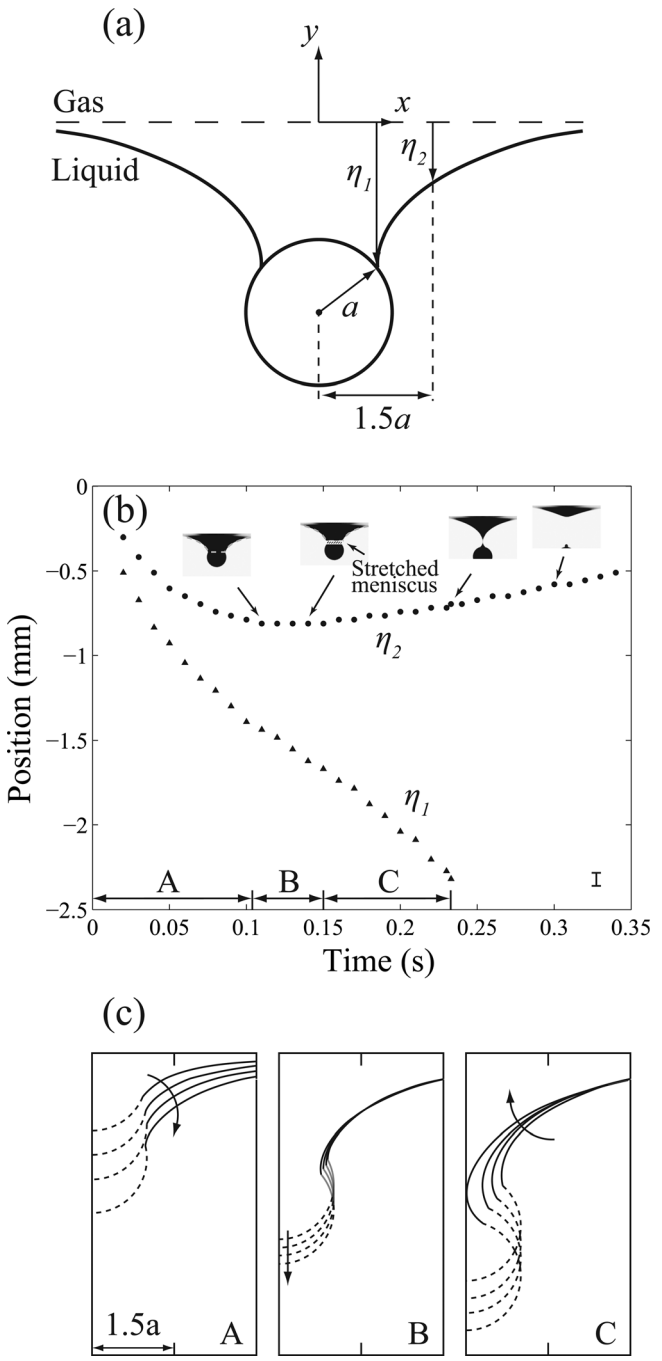

FIG. 7. (a) Schematic of a sphere straddling a gas-liquid interface. (b) The temporal evolution of the vertical positions of the contact line (triangles) and the meniscus at $x = 1.5a$ (circles) for a sphere of Fig. 4(b). A characteristic error bar is shown. (c) Temporal evolution of the meniscus (black line) and a wet part of the sphere (dashed line). Time increases in the direction of the arrow taking the values 0.020, 0.032, 0.049, and 0.080 s (time range A); 0.111, 0.122, 0.133, and 0.145 s (time range B); and 0.168, 0.192, 0.212, and 0.233 s (time range C).

corresponding points in Fig. 4. We see that both the diamond (result of free energy analysis) and the triangle (result of ϕ_0 condition) occur before the complete immersion of the sphere. This implies that the sinking sphere and surrounding fluid reach a lower energy state than the completely immersed system and that ϕ_0 exceeds $\pi/2$, implying that a neck occurs between the sphere and the undisturbed free surface. The meniscus is observed to be detached from the sphere when the neck closes. Analysis of the unstable snapping process of the meniscus is also important in predicting the failure of the liquid bridges connecting two solid objects or a faucet and a falling drop,[18,19,22] a mirror system to our problem. Resolution of this issue in general requires intensive numerical computations[23–25] and consideration of inertial effects,[26] a topic not further pursued here.

C. Scaling law for sinking time

Figures 4(a) and 4(b) both show that the sphere sinks with a rather constant velocity for a relatively long duration ($\sim 0.2 < t <\sim 0.8$ s in (a) and $\sim 0.05 < t <\sim 0.23$ s in (b)) after a fast fall in the beginning. Since the sphere falls at a constant rate for most of the sinking time, estimating this steady velocity can give the characteristic sinking time. For the steady sinking interval, the solid weight is dominantly balanced by the surface tension force, F_s, and the viscous drag, F_d (F_b is negligible as can be checked in Fig. 5). For a sphere, the maximum value of F_s can be estimated as[2] $F_s \approx 2\pi a\gamma \sin^2(\theta/2)$. For drag, we approximate $F_d \approx 6\pi\mu U_s a$, where U_s denotes the constant sinking speed, because a

significant portion of the sphere area is wet by liquid in the steady-velocity region. The force balance $F_d = F_w - F_s$ leads to

$$\mathrm{Ca_s} = \frac{2}{9}D\mathrm{Bo} - \frac{1}{3}\sin^2\left(\frac{\theta}{2}\right), \tag{17}$$

where the nondimensional velocity $\mathrm{Ca_s} = \mu U_s/\gamma$ is linearly proportional to DBo but lower than that of a fully immersed sphere by $\frac{1}{3}\sin^2(\theta/2)$. Figure 8(a) shows a plot of $\mathrm{Ca_s}$ versus DBo to compare the theory with experiments. The solid lines I and II plot Eq. (17) with the lower and upper bounds of θ observed in the experiments, 120° and 150°, respectively. We see that all the experimental results lie between the two lines. The dashed line corresponds to the steady velocity of a fully immersed sphere.

Using U_s, we can predict the characteristic sinking time, t_s, taken for a sphere to get completely immersed in liquid. The sinking depth, h_d, a vertical distance from the unperturbed free surface that the sphere should travel before losing its contact with the meniscus, is experimentally found to be linearly proportional to the sphere radius for each liquid: $h_d \sim a$. Because $t_s \sim h_d/U_s$, we get the following relation for the nondimensional sinking time $\tau_s = t_s\gamma/(\mu a)$:

$$\tau_s \sim \mathrm{Ca_s}^{-1} = \left[\frac{2}{9}D\mathrm{Bo} - \frac{1}{3}\sin^2\left(\frac{\theta}{2}\right)\right]^{-1}. \tag{18}$$

Figure 8(b) shows that the experimentally measured sinking times (from the first contact to the complete immersion) follow our scaling law as their dimensionless values collapse onto a straight line with a slope 2.39. In physical terms, it takes longer for a sphere to sink as the liquid viscosity and surface tension and the contact angle increase, and as the sphere density and radius decrease. But, we note that the liquid density plays an insignificant role in sinking of small objects (Bo $\ll$ 1) because of small contribution of hydrostatic pressure force.

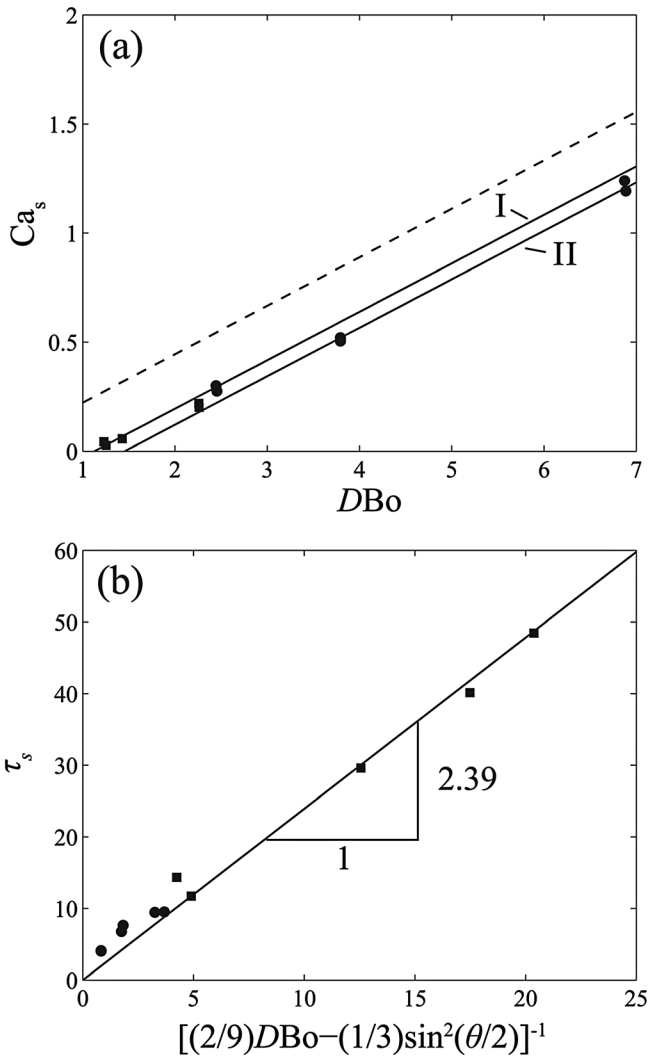

FIG. 8. (a) The capillary number based on the steady sinking velocity, $\mathrm{Ca_s}$ versus DBo. The solid and dashed lines are theoretical results. (b) The sinking times τ_s plotted according to the scaling law (18). The best fitting straight line has the slope 2.39. Squares and circles correspond the experimental results in glycerine and silicone oil, respectively.

IV. CONCLUSIONS

Our experimental and theoretical analyses enabled us to calculate the velocity of a tiny sphere sinking into a viscous liquid. Also a scaling law was developed to predict the characteristic sinking time as the function of the material properties and dimensions. To further understanding of the entire process of sinking, it is natural to ask what happens in the late stage when the meniscus becomes unstable and eventually snaps. Despite a number of studies in the pinching of a liquid bridge, relatively few studies have been reported on the snapping of a meniscus following a solid object penetrating an air-liquid interface. More detailed analysis on this topic combined with sophisticated numerical analysis is called for. Based on the understanding of two limiting situations of the sinking, i.e., inertia dominant sinking[13,27] and viscosity dominant sinking (treated here), it will be of interest to consider both the inertial and viscous effects to solve the dynamics with an intermediate Re. In relation to the biological implication of this problem, the sinking dynamics on a viscoelastic liquid is worth for further study because the viscoelasticity of the fluid contained in a pitcher plant is known to play a crucial role in the insect-trapping function of the carnivorous plant.[8]

ACKNOWLEDGMENTS

This work was supported by the National Research Foundation of Korea (Grant Nos. 2009-0076168 and 412-J03001) and administered via SNU-IAMD.

APPENDIX: CONDITION FOR COMPLETE IMMERSION USING FREE ENERGY ANALYSIS

From the viewpoint of free energy, we may anticipate that upon complete immersion, the difference of the free energy E of the sinking system from that of the immersed state (E_f) vanishes: $E - E_f = 0$. When a sphere sinks, the total free energy change is the sum of the free energy change due to the changes of the interfacial areas of the liquid with the solid (ΔE_1) and with the air (ΔE_2) and the changes of the gravitational potential energy of the liquid (ΔE_3) and of the sphere (ΔE_4). Here, ΔE represents the difference of E and

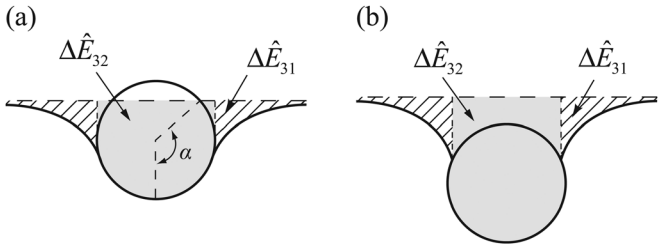

FIG. 9. The cross-sectional view of the liquid depressed by the sphere for (a) $|h_0| \leq a$ and (b) for $|h_0| > a$.

that of the reference state E_r corresponding to the sphere just touching the gas-liquid interface: $\Delta E = E - E_r$. In the following, we nondimensionalize the energy with γa^2, thus, $\hat{E} = E/(\gamma a^2)$. The free energy change due to the increase of the wetted area is written as

$$\Delta\hat{E}_1 = -2\pi(1 - \cos\beta)\cos\theta. \tag{A1}$$

The free energy change associated with the change of the air-liquid interfacial area is

$$\Delta\hat{E}_2 = \frac{2\pi}{\mathrm{Bo}}\int_{\phi_0}^{0} X(\sec\phi - 1)\left(\frac{\mathrm{d}X}{\mathrm{d}\phi}\right)\mathrm{d}\phi - \pi\sin^2\beta, \tag{A2}$$

where $X = x/l_c$. The work required to depress the liquid weight displaced by the meniscus, represented as the hatched region in Fig. 9, is written as $\Delta\hat{E}_{31}$,

$$\Delta\hat{E}_{31} = \frac{\pi}{\mathrm{Bo}}\int_{\phi_0}^{0} XY^2\left(\frac{\mathrm{d}X}{\mathrm{d}\phi}\right)\mathrm{d}\phi,$$

where

$$Y = y/l_c. \tag{A3}$$

The free energy change associated with the work required to depress the liquid underneath the sphere bounded by the wetted surface of the solid, a vertical cylinder through the contact line, and the unperturbed free surface represented as the gray area in Fig. 9 is

$$\begin{aligned}\Delta\hat{E}_{32} = \pi\mathrm{Bo}\Bigg[&\frac{1}{2}\cos^2\alpha(\sin^2\beta - \sin^2\alpha + 1)\\ &+\frac{1}{3}\cos\alpha(\cos^3\beta - \cos^3\alpha - 2)\\ &-\frac{1}{4}(\cos^4\beta - \frac{2}{3}\cos^4\alpha - 1)\Bigg]\end{aligned} \tag{A4}$$

for $|h| \leq a$ and

$$\begin{aligned}\Delta\hat{E}_{32} = \pi\mathrm{Bo}\Bigg[&\frac{1}{2}\left(\frac{H}{R}\right)^2(1-\cos^2\beta) + \frac{2H}{3R}(-1+\cos^3\beta)\\ &+\frac{1}{4}(1-\cos^4\beta)\Bigg]\end{aligned} \tag{A5}$$

for $|h| > a$, where α is the angular position at which the original free surface intersects the sphere, $H = h/l_c$, and $R = a/l_c$. The total work done associated with depressing liquid is $\Delta\hat{E} = \Delta\hat{E}_{31} + \Delta\hat{E}_{32}$. The change of gravitational potential energy of the sphere is

$$\Delta\hat{E}_4 = \frac{4}{3}\pi D\mathrm{Bo}(\cos\alpha - 1) \tag{A6}$$

for $|h| \leq a$ and

$$\Delta\hat{E}_4 = \frac{4}{3}\pi D\mathrm{Bo}\left(\frac{H}{R} - 1\right) \tag{A7}$$

for $|h| > a$.

Now the total free energy change for the sinking sphere is

$$\Delta\hat{E} = \Delta\hat{E}_1 + \Delta\hat{E}_2 + \Delta\hat{E}_3 + \Delta\hat{E}_4. \tag{A8}$$

For a fully immersed sphere, the free energy difference is written as

$$\Delta\hat{E}_f = -4\pi\cos\theta - \frac{4}{3}\pi HR + \frac{4}{3}\pi D\mathrm{Bo}\left(\frac{H}{R} - 1\right). \tag{A9}$$

The first term on the right hand side of Eq. (A9) corresponds to the work required to fully wet the solid surface with liquid, the second term is the work required to displace the volume of liquid occupied by the solid, and the last term is the gravitational potential energy difference of the solid. In our computation, we calculate $\Delta\hat{E} - \Delta\hat{E}_f$ for each time step to find the instant when $E = E_f$, which is indicated as a diamond in Fig. 4.

[1]J. B. Keller, "Surface tension force on a partly submerged body," Phys. Fluids **10**, 3009 (1998).
[2]D. Vella, D.-G. Lee, and H.-Y. Kim, "The load supported by small floating objects," Langmuir **22**, 5979 (2006).
[3]D. Vella, "Floating objects with finite resistance to bending," Langmuir **24**, 8701 (2008).
[4]K. J. Park and H.-Y. Kim, "Bending of floating flexible legs," J. Fluid Mech. **610**, 381 (2008).
[5]B. V. Derjaguin and S. S. Dukhin, "Theory of flotation of small and medium-size particles," Trans. Inst. Min. Metall. **70**, 221 (1961).
[6]J. W. M. Bush and D. L. Hu, "Walking on water: Biolocomotion at the interface," Annu. Rev. Fluid Mech. **38**, 339 (2006).
[7]R. B. Suter, "Cheap transport for fishing spiders (Araneae, Pisauridae): The physics of sailing on the water surface," J. Arachnol. **27**, 489 (1999).
[8]L. Gaume and Y. Forterre, "A viscoelastic deadly fluid in carnivorous pitcher plants," PLoS ONE **2**, e1185 (2007).
[9]D. Vella, D.-G. Lee, and H.-Y. Kim, "Sinking of a horizontal cylinder," Langmuir **22**, 2972 (2006).
[10]D. Vella and J. E. Li, "The impulsive motion of a small cylinder at an interface," Phys. Fluids **22**, 052104 (2010).
[11]C. Duez, C. Ybert, C. Clanet, and L. Bocquet, "Making a splash with water repellency," Nat. Phys. **3**, 180 (2007).
[12]J. M. Aristoff and J. W. M. Bush, "Water entry of small hydrophobic spheres," J. Fluid Mech. **619**, 45 (2009).
[13]D.-G. Lee and H.-Y. Kim, "Impact of a superhydrophobic sphere onto water," Langmuir **24**, 142 (2008).
[14]H. J. Schulze, "New theoretical and experimental investigations on stability of bubble/particle aggregates in flotation: A theory on the upper particle size of floatability," Int. J. Min. Process. **4**, 241 (1977).
[15]G. I. Taylor and D. H. Michael, "On making holes in a sheet of fluid," J. Fluid Mech. **58**, 625 (1973).
[16]S. Gaudet, G. H. McKinley, and H. A. Stone, "Extensional deformation of Newtonian liquid bridges," Phys. Fluids **8**, 2568 (1996).
[17]D.-G. Lee and H.-Y. Kim, "The role of superhydrophobicity in the adhesion of a floating cylinder," J. Fluid Mech. **624**, 23 (2009).
[18]J. F. Padday, G. Petre, C. G. Rusu, J. Gamero, and G. Wozniak, "The shape, stability and breakage of pendant liquid bridges," J. Fluid Mech. **352**, 177 (1997).
[19]M. A. Erle, D. C. Dyson, and N. R. Morrow, "Liquid bridges between cylinders, in a torus, and between spheres," AIChE J. **17**, 115 (1971).

[20]G. G. Stokes, "On the effect of the internal friction of fluids on the motion of pendulums," Trans. Cambridge Philos. Soc. **9**, 8 (1851).
[21]G. K. Batchelor, *An Introduction to Fluid Dynamics* (Cambridge University Press, Cambridge, UK, 1967).
[22]B. A. Qian and K. S. Breuer, "The motion, stability and breakup of a stretching liquid bridge with a receding contact line," J. Fluid Mech. **666**, 554 (2011).
[23]J. Eggers and T. F. Dupont, "Drop formation in a one-dimensional approximation of the Navier-Stokes equation," J. Fluid Mech. **262**, 205 (1994).
[24]X. D. Shi, M. P. Brenner, and S. R. Nagel, "A cascade of structure in a drop falling from a faucet," Science **265**, 219 (1994).
[25]J. Eggers, "Nonlinear dynamics and breakup of free-surface flows," Rev. Mod. Phys. **69**, 865 (1997).
[26]R. Kröger, S. Berg, A. Delgado, and H. J. Rath, "Stretching behaviour of large polymeric and Newtonian liquid bridges in plateau simulation," J. Non-Newtonian Fluid Mech. **45**, 385 (1992).
[27]J. M. Aristoff, T. T. Truscott, A. H. Techet, and J. W. M. Bush, "The water entry of decelerating spheres," Phys. Fluids **22**, 032102 (2010).